



Multuser Parallel Transmission with 1-Tap Time Domain Beamforming by Millimeter Wave Massive Antenna Arrays

By Kazuki Maruta, Atsushi Ohta, Takuto Arai, Tatsuhiko Iwakuni, Yushi Shirato,
Satoshi Kurosaki & Masataka Iizuka

Nippon Telegraph and Telephone Corporation

Abstract- This paper investigates the feasibility of multuser parallel transmission by sub-array beamforming using millimeter wave bands in which the Line-of-Sight (LoS) dominant channel environment is expected. Focusing on high beamforming gain provided by the massive antenna array, each sub-array conducts first eigenmode transmission and thus one stream is allocated per user without null steering. This paper also proposes 1-tap time domain beamforming (TDBF) as the same weight is applied to all frequency components.

Keywords: *massive antennas, sub-array, first eigenmode, time domain beamforming, parallel transmission. Milli meter wave.*

GJCST-A Classification : *D.4.4, C.1.4*



Strictly as per the compliance and regulations of:



Multiuser Parallel Transmission with 1-Tap Time Domain Beamforming by Millimeter Wave Massive Antenna Arrays

Kazuki Maruta ^α, Atsushi Ohta ^σ, Takuto Arai ^ρ, Tatsuhiko Iwakuni ^ω,
Yushi Shirato [¥], Satoshi Kurosaki [§] & Masataka Iizuka ^χ

Abstract- This paper investigates the feasibility of multiuser parallel transmission by sub-array beamforming using millimeter wave bands in which the Line-of-Sight (LoS) dominant channel environment is expected. Focusing on high beamforming gain provided by the massive antenna array, each sub-array conducts first eigenmode transmission and thus one stream is allocated per user without null steering. This paper also proposes 1-tap time domain beamforming (TDBF) as the same weight is applied to all frequency components. It reduces computation complexity as well as suppressing the effect of additive noise on weight derivation. Computer simulation results show that increasing the sub-array spacing stably improves signal-to-interference power ratio (SIR) performance and that the proposed 1-tap TDBF can match the performance of the frequency domain first eigenmode transmission as a rigorous solution.

Keywords: massive antennas, sub-array, first eigenmode, time domain beamforming, parallel transmission. Millimeter wave.

1. INTRODUCTION

The rapid spread of wireless communication devices such as smartphones and tablets has triggered diversification in mobile services. Not only is data traffic exploding, but also large numbers of terminals are crowding key sites such as station, airports and event venues. Unfortunately, frequency resources are being depleted rapidly, especially in the microwave band since many kinds of wireless communication systems such as wireless fidelity (Wi-Fi), worldwide interoperability for microwave access (WiMAX) or long-term evolution (LTE) (-Advanced) have become voracious consumers. Overcoming this shortfall is a critical issue in wireless communication. Drastic improvements in transmission rate and system capacity are required towards 5th generation mobile communications (5G) [1]. Promising solutions [2, 3] include micro-cells for area spectral efficiency improvement and exploiting millimeter wavebands such as super high frequency (SHF) or extremely high frequency (EHF) bands where rich spectrum resources are available. The main problem in using millimeter wavebands is the link budget shortfall. The propagation

loss is high and the performance of radio frequency (RF) components such as high power amplifier (HPA) is limited in millimeter wavebands.

The application of massive multiple-input multiple-output (MIMO) [4-7] is one of the most promising solutions. Massive MIMO can provide large beamforming gain with huge numbers of arrayed antenna elements without high-performance high-cost RF components [8]. In addition, higher order space division multiplexing (SDM) can be applied by using its excess degree of freedom (DoF) to enhance the transmission rate. It is noted that higher order SDM divides total transmission power but the beamforming gain should be sufficient to perform SDM. The beamforming gain is, ideally, given by $10\log_{10}(NtNr)$ dB, where Nt and Nr are the numbers of transmission and reception antenna elements, respectively. This means that increasing the number of antenna elements from 100 to 200 yields a gain of only 3 dB making arrays with more than 100 elements not cost effective. If the link budget is insufficient with the use of around 100 elements, we have only two options; one is limiting the service area to reduce the propagation loss and the other is employing directional antennas to attain larger antenna gain. A high-functionality base station (BS) with massive array is expensive making quite small service areas unacceptable from the operating viewpoint. On the other hand, the use of directional antennas raises the correlation of the antenna elements of user equipment (UE). This results in a large level gap between the 1st and 2nd eigenvalues which hinders higher order SDM application [9]. Moreover, the feasibility of higher order SDM in actual environments has not been confirmed for future BSs and UEs with practical specifications. From the above background, this paper discusses a different approach to exploiting massive element numbers with Line-of-Sight (LoS) dominant channels.

The next promising approach to obtain higher system capacity, multiuser MIMO [10], spatially multiplexes the UEs to use the same frequency channel at the same time. As described above, channel environments in millimeter wavebands are considered to be dominated by the LoS component since BS and/or

Author ^α ^σ ^ρ ^ω [¥] [§] ^χ: NTT Access Network Service Systems Laboratories, Nippon Telegraph and Telephone Corporation, Yokosuka-shi, 239-0847 Japan. e-mail: maruta.kazuki@lab.ntt.co.jp

UEs are required to have highly directive antennas in order to obtain adequate transmission/reception performance. In such situation, multiuser diversity gain is expected to increase the system capacity [9, 11] since the inter-user correlation between UEs is lower than intra-user correlation. In other words, it can be a promising solution for the problem of the large level gap between the 1st and 2nd eigenvalues in the LoS dominant channel for a single user MIMO. Meanwhile, to spatially multiplex several UEs, the BS requires channel state information at the transmitter (CSIT) to suppress inter-user interference (IUI). The accuracy of CSIT is degraded by the channel time variation created by movement of the UEs or objects around the UEs. Inaccurate CSIT causes incomplete IUI suppression which degrades the signal-to-interference power ratio (SIR) performance of multiuser MIMO [12]. We have verified one of the massive MIMO benefits; the improved robustness of multiuser transmission in time varying channel environments [13]. The gain of the beamforming provided by a massive array is concentrated on the target UE and the average level of IUI leakage in the space is adequately suppressed. This causes high energy efficiency and minimal IUI leakage between the multiplexed UEs even with user movement. From the above features, we are focusing on multiuser massive MIMO which allocates only 1st eigenmode to each UE to achieve stable and enhanced system capacity even in high mobility situations [9]. Given the LoS environment, 1st eigenvalue usage is outstandingly effective since its transmission/reception beams are much more stable than those for 2nd and higher order eigenmodes. However, block diagonalization (BD) or singular value decomposition (SVD) computations of large-scale matrices for each frequency component incur quite heavy computation loads given the assumption of millimeter wideband transmission. The effective solution of hybrid analog/digital beamforming has been studied [8, 14-17]. Analog beamforming can reduce costly RF chains and the computation costs associated with digital processing. It requires beam training or search with the use of pre-determined beam patterns, which imposes some overhead. In the 5G world, it is expected that the number of accommodated UEs in a cell will become larger and it may makes the overhead heavy. These are the reasons why a breakthrough in simplified massive MIMO operation is required.

This paper first investigates the feasibility of multiuser parallel transmission via isolated sub-arrays (SAs). BS uses multiple SAs that are separated from each other and only 1 signal stream per SA is allocated to each UE via 1st eigenmode without null steering. This elimination of signal processing for null steering eases the total computation load. The isolation of all transmission and reception points from each other helps to ensure low correlated channels so null steering is not

necessary. Second, we introduce 1-tap time domain beamforming (TDBF) to drastically alleviate this calculation cost. TDBF weight can be determined by simply correlating reception signals between antenna elements, which basically corresponds to extracting the strongest path, i.e., the LoS component. When SA is a narrow-spaced array (e.g. half-wavelength), incoming direct wave signals are regarded as plane waves. In this case, the frequency dependence of the weight is limited and it is possible to employ constant weights in the frequency domain. As a result, the 1-tap TDBF weight can be applied to all frequency components. Furthermore, it can be obtained under very low SNR conditions, less than 0 dB, without beamforming. Assuming that we assign a single stream to each SA and UE, the signal processing for TDBF can be significantly simplified even though full digital signal processing is employed and hardware resource requirements can be minimized with optimized designs. The contributions of this paper are: 1) The SIR performance of SA beamforming is revealed for the parameters of SA spacing, SA antenna element number, Rician K -factor, and UE movement speed. 2) A 1-tap TDBF scheme is presented and its effectiveness is verified.

The rest of this paper is organized as follows. Section 2 defines the system model and presents the methodology of multiuser parallel transmission by the sub-arrayed BS configuration. Section 3 describes the 1-tap TDBF scheme. Computer simulation results are provided in Section 4. Finally, Section 5 concludes the paper. Throughout the paper, normal letters represent scalar quantities, bold lowercase letters indicate vectors and uppercase letters indicate matrices. $|\cdot|$, $(\cdot)^*$, $(\cdot)^T$, and $(\cdot)^H$ represent absolute values, conjugate values, transpose and conjugate transpose, respectively.

II. SYSTEM DEFINITION

a) System and Channel Model

The system model is depicted in Fig. 1. BS is composed of N_a SAs, each of which has N_t elements in a uniform planar array (UPA). SA serves one UE with N_r

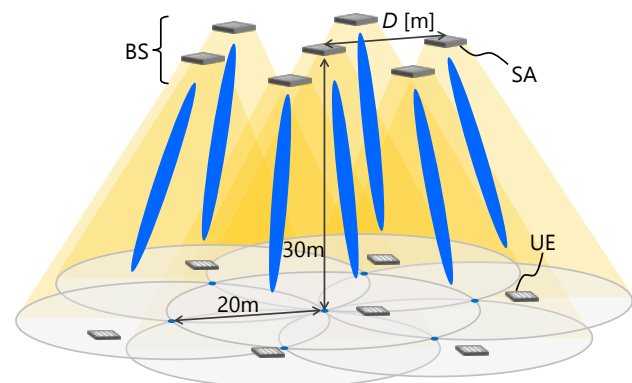


Figure 1 : System model

UPA elements via beamforming; only a single stream is allocated to each UE. To ensure the LoS environment and reduce the probability of human blockage [18], SAs should be installed at high positions. To provide a simple evaluation of the potential of the proposed method, BS is assumed to be ceiling mounted and UEs face straight up as shown in Fig. 1. This scenario can be realized at stadiums and large halls like exhibition centers, and simple variants will support different situations such as installation of the walls of buildings. Fig. 1 shows a typical case for a simple feasibility study. Assuming multicarrier transmission such as orthogonal frequency division multiplexing (OFDM), we define the channel matrix per subcarrier, $\mathbf{H} \in \mathbb{C}^{Nu \times Na}$, as follows;

$$\mathbf{H} = [\mathbf{H}_1^T \ \dots \ \mathbf{H}_i^T \ \dots \ \mathbf{H}_{Nu}^T]^T \quad (1)$$

$$\mathbf{H}_i = [\mathbf{H}_{i1} \ \dots \ \mathbf{H}_{ij} \ \dots \ \mathbf{H}_{iNa}] \quad (2)$$

where $\mathbf{H}_i \in \mathbb{C}^{Nr \times Na}$ denotes the channel sub matrix between the i -th UE and BS. Note that these expressions are per subcarrier and indices have been omitted. A Rician fading channel is considered so \mathbf{H}_i is expressed using Rician K -factor as,

$$\mathbf{H}_i = \sqrt{\frac{K}{K+1}} \mathbf{H}_{LoS,i} + \sqrt{\frac{1}{K+1}} \mathbf{H}_{NLoS,i} \quad (3)$$

$\mathbf{H}_{LoS,i}$ is determined by the spatial relationship of the i -th UE and BS;

$$\mathbf{H}_{LoS,i} = \frac{\lambda}{4\pi} \begin{bmatrix} \frac{e^{-j2\pi \frac{d_{11}}{\lambda}}}{d_{11}} & \dots & \frac{e^{-j2\pi \frac{d_{1(NaNt)}}{\lambda}}}{d_{1(NaNt)}} \\ \vdots & \ddots & \vdots \\ \frac{e^{-j2\pi \frac{d_{mn}}{\lambda}}}{d_{mn}} & \dots & \frac{e^{-j2\pi \frac{d_{Nr(NaNt)}}{\lambda}}}{d_{Nr(NaNt)}} \\ \vdots & \ddots & \vdots \\ \frac{e^{-j2\pi \frac{d_{Nr1}}{\lambda}}}{d_{Nr1}} & \dots & \frac{e^{-j2\pi \frac{d_{Nr(NaNt)}}{\lambda}}}{d_{Nr(NaNt)}} \end{bmatrix} \quad (4)$$

where d_{mn} is the distance between the m -th antenna element of i -th UE and the n -th BS antenna element. λ is the carrier wavelength. The channel time variation of $\mathbf{H}_{LoS,i}$ is simulated by the spatial relationships between the UEs and the BSs as determined by UE movement. $\mathbf{H}_{NLoS,i}$ is the non-line-of-sight (NLoS) component from the scatters, which are uniformly sited around the UEs. Each element of $\mathbf{H}_{NLoS,i}$ also includes a path loss coefficient of $\lambda/(4\pi d_{mn})$. To consider the spatial correlation between BS antenna elements, independent identically distributed (i.i.d.) Rayleigh fading channels are converted into correlated channels using the Kronecker model [19]

$$\mathbf{H}_{NLoS,i} = \mathbf{R}_{rx,i}^{1/2} \mathbf{H}_{iid,i} (\mathbf{R}_{tx,i}^{1/2})^T \quad (5)$$

where $\mathbf{R}_{tx,i} \in \mathbb{C}^{Nr \times Nr}$, $\mathbf{R}_{rx,i} \in \mathbb{C}^{Nu \times Nu}$ are correlation matrices [20]. Assuming the 3GPP 3D channel model [21], the half power beamwidth (HPBW) of each antenna element is set to 65°. The power azimuth spectrum (PAS) of an arriving path at the base station is assumed to have a Laplacian distribution [22] and its deviation value is set to 5°. Time variation of the NLoS component follows Jakes' model [23].

b) *Sub-Array Multiuser Parallel Transmission by First Eigenmode*

The i -th UE obtains a sub-block channel matrix to the i -th SA, $\mathbf{H}_i \in \mathbb{C}^{Nr \times Na}$, and computes the SVD [10].

$$\mathbf{H}_i = [\mathbf{u}_i \ \bar{\mathbf{U}}_i] \mathbf{\Sigma}_i [\mathbf{v}_i^H \ \bar{\mathbf{V}}_i^H] \quad (6)$$

where $\mathbf{u}_i \in \mathbb{C}^{Nr \times 1}$ and $\mathbf{v}_i \in \mathbb{C}^{Na \times 1}$ represent left and right singular vectors corresponding to the 1st eigenmode, respectively. $\mathbf{\Sigma}_i \in \mathbb{C}^{Nr \times Na}$ is a singular value matrix whose diagonal elements are arranged in descending order. With the LoS dominant channel, it is expected that the 1st eigenmode weight vectors \mathbf{u}_i^H and \mathbf{v}_i attain beamforming gain by extraction of the LoS component. Denoting the transmission signal vector of all UE/SAs as $\mathbf{T} = [t_1, \dots, t_i, \dots, t_{Nu}]^T \in \mathbb{C}^{Nu \times 1}$, reception signal vector, $\mathbf{Y} = [y_1, \dots, y_i, \dots, y_{Nu}]^T \in \mathbb{C}^{Nu \times 1}$, is expressed as follows;

$$\mathbf{Y} = \begin{bmatrix} \mathbf{u}_1^H & & \mathbf{O} \\ & \ddots & \\ \mathbf{O} & & \mathbf{u}_{Na}^H \end{bmatrix} \mathbf{H} \begin{bmatrix} \mathbf{v}_1 & & \mathbf{O} \\ & \ddots & \\ \mathbf{O} & & \mathbf{v}_{Na} \end{bmatrix} \mathbf{T} + \mathbf{n} \quad (7)$$

where \mathbf{n} is an additive white Gaussian noise (AWGN) vector. It should be noted that $Na = Nu$. The i -th UE and SA perform beamforming only to each other as an isolated system and do not care about the other j -th ($i \neq j$) UE/SA pairs. If SAs are spatially de-correlated with large enough inter-SA spacing, significant SIR gain can be expected without null steering. SIR and SINR for the i -th UE are given by;

$$\text{SIR}_i = 10 \log_{10} \frac{|\mathbf{u}_i^H \mathbf{H}_{ii} \mathbf{v}_i|^2}{\sum_{j=1, j \neq i}^{Na} |\mathbf{u}_i^H \mathbf{H}_{ij} \mathbf{v}_j|^2} \quad (8)$$

$$\text{SINR}_i = 10 \log_{10} \frac{|\mathbf{u}_i^H \mathbf{H}_{ii} \mathbf{v}_i|^2}{\sum_{j=1, j \neq i}^{Na} |\mathbf{u}_i^H \mathbf{H}_{ij} \mathbf{v}_j|^2 + \sigma^2} \quad (9)$$

where σ^2 is the noise variance defined as single-input single-output (SISO) situation.

III. 1-TAP TIME DOMAIN BEAMFORMING

First of all, we have set up a hypothesis for the LoS dominant channel such that the first eigenmode

reception weight can be approximately obtained as the simple reception weight determined for the case in which only a single antenna element located around the center of the array antenna at UE side transmits a training signal for channel estimation. Though it is done in a quite low SNR condition because of the link budget shortfall, the subsequent application of TDBF makes accurate weight estimation under such condition possible. After obtaining an adequate transmission weight at BS side, UE can easily obtain the MRC reception weight by receiving training signal transmitted from SA at BS side with the transmission weight. In millimeter wave communication, inter-element spacing becomes much smaller than BS-UE distance. In the case of Fig. 1, BS uses a directional antenna to improve the link budget, so angle-of-departure (AoD) and/or angle-of-arrival (AoA) at BS side is quite small. In this case, when we observe relative phase information to the reference antenna element, in-band phase fluctuation is not so huge whereas the individual phase information fluctuates largely with bandwidth. The individual phase information is given by $2\pi d_m f/c$ where d_m is the distance between transmission/reception antennas, f is the carrier frequency and c is the light speed. Meanwhile, the relative phase information of the m -th antenna element is given by $2\pi \Delta d_m f/c$ where Δd_m is the path length difference between the m -th antenna element and the reference antenna element (e.g. the 0-th element), i.e. $\Delta d_m = d_m - d_0$. Here, $d_m \gg \Delta d_m$ and $2\pi \Delta d_m f/c$ is negligible [9]. Note that the beamforming weight is determined by the relative CSI instead of absolute CSI; common phase offset for all elements is not important. The stable relative phase information enables us to apply the same beamforming weight for all frequency components. Fourier transformation of the constant weight in the frequency domain yields an impulse shaped tap coefficient in the time domain, i.e. a 1-tap TDBF weight. Though clearly a simplified scheme, it can still strengthen the dominant arriving path.

Fig. 2 overviews the proposed 1-tap TDBF. First, a training signal is transmitted from one UE antenna element at the UPA's center. Received signal for the m -th antenna element ($m = 0, 1, \dots, N_t-1$) of SA, $\mathbf{x}_m \in \mathbb{C}^{N_s \times 1}$, is expressed as;

$$\mathbf{x}_m = \begin{bmatrix} h_m[0] & 0 & & h_m[L-1] & & h_m[1] & & & \\ h_m[1] & h_m[0] & \ddots & 0 & \ddots & \vdots & & & \\ \vdots & h_m[1] & & \vdots & & h_m[L-1] & & & \\ h_m[L-1] & \vdots & & 0 & & \vdots & & & \\ 0 & h_m[L-1] & & 0 & & \vdots & & & \\ 0 & 0 & \ddots & h_m[0] & \ddots & \vdots & & & \\ \vdots & \vdots & & h_m[1] & & 0 & & & \\ 0 & 0 & & \vdots & & h_m[0] & & & \end{bmatrix} \begin{bmatrix} s_0 \\ s_1 \\ \vdots \\ s_{N_s-1} \end{bmatrix} + \begin{bmatrix} n_0 \\ n_1 \\ \vdots \\ n_{N_s-1} \end{bmatrix} \quad (10)$$

Note that this is a time domain expression. N_s represents the sample number of the training signal.

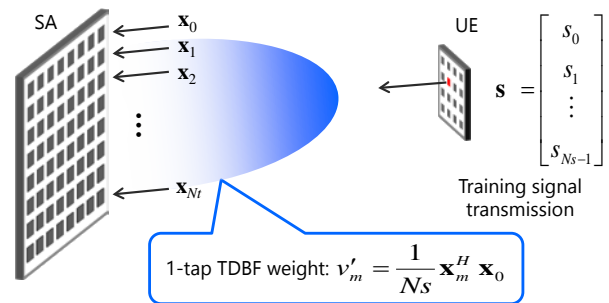


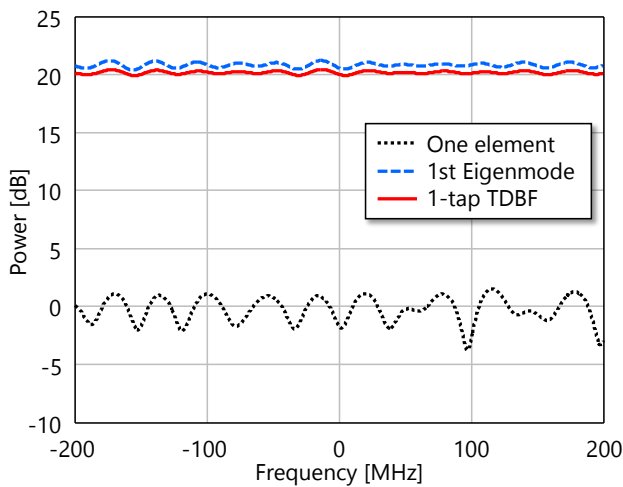
Figure 2 : Proposed 1-tap TDBF

$h_m[l]$ is the l -th ($l = 0, \dots, L-1$) complex path gain of the channel impulse response for the m -th reception antenna element of SA. L denotes the number of paths. s_α and n_α ($\alpha = 0, \dots, N_s-1$) are training signal samples and AWGN components in the time domain, respectively. Eq. (10) assumes cyclic prefix insertion. SA then calculates the maximal ratio combining (MRC) weight [24], \mathbf{v}'_m , by correlating the signals received on the m -th and reference antenna elements (here assumes $m = 0$), in the time domain.

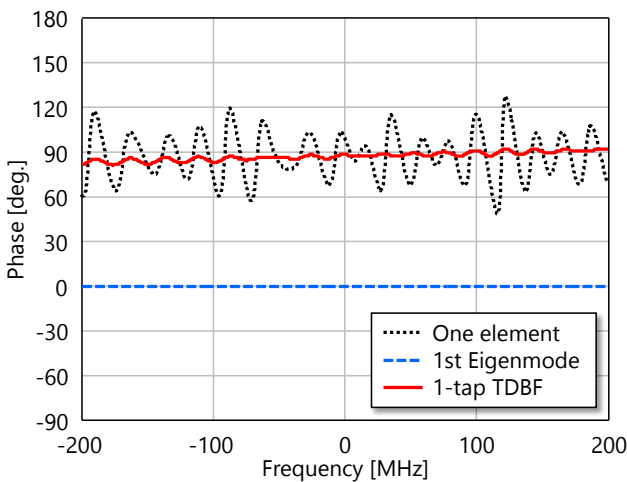
$$\mathbf{v}'_m = \frac{1}{N_s} \mathbf{x}_m^H \mathbf{x}_0 \quad (11)$$

TDBF reception weight vector for the i -th SA, $\mathbf{v}'_i = [v'_{i0}, \dots, v'_{im}, \dots, v'_{iN_t-1}] \in \mathbb{C}^{N_t \times 1}$, is obtained. Note that reciprocity calibration [25, 26] is required to obtain the transmission weight from the reception weight since uplink and downlink signals go through different circuits. This paper assumes that the processing is ideal. Eq. (11) can suppress the additive noise effect since the received signals for each sample are correlated whereas the noise components are identically independent in the samples. When $N_s = 1000$ for example, the signal-to-noise power ratio (SNR) can be improved 30 dB and weight accuracy is greatly improved. The weight calculation can work correctly even in low SNR conditions with link budget shortfall and is one of advantages of the 1-tap TDBF scheme. Finally, SA applies the TDBF weight and transmits a training signal to UE. In this process, the SA works as a single virtual antenna with large beamforming gain due to the TDBF weight. Owing to this gain, UE estimates the equivalent channel vector for the virtual single antenna, $\mathbf{H}_i \mathbf{v}'_i \in \mathbb{C}^{N_r \times 1}$ under the improved SNR condition; it can be utilized as MRC weight vector, $\mathbf{u}'_i{}^H = (\mathbf{H}_i \mathbf{v}'_i)^H$. When BS is composed of multiple SAs, UE identification, e.g. which SA is allocated to which UE, can be controlled by BS in a centralized manner.

To understand the fundamental performance of TDBF, we first evaluate the single antenna UE case in which SA with 121 elements UPA performs TDBF to UE with 1 antenna element. Fig. 3 shows an example of the power and phase spectra. In this figure, red, blue and black lines show the results for proposed 1-tap TDBF,



(a) Power spectrum.



(b) Phase spectrum.

Figure 3: Fundamental performance of 1-tap TDBF

1st eigenmode, and one element without beamforming, respectively. This evaluation assumes the Rician channel model with $K = 10$ dB and 16 scatterers are located around UE. The 1st eigenmode transmission, which is equal to maximal ratio transmission (MRT) in this case, is performed for each subcarrier. It attains the beamforming gain calculated as $10\log_{10}(121) = 20.8$ dB, as shown in Fig. 3 (a). Meanwhile, 1-tap TDBF achieves comparable beamforming performance; the difference is only about 1 dB. It is clear that both beamforming arrangements can compensate the channel distortion unlike the single antenna reception case. When we observe Fig. 3 (b), the phase spectrum without beamforming (i.e. SISO) fluctuates by about 60° due to the multipath components. The 1st eigenmode transmission cancels this fluctuation to 0° . Phase components and frequency components are perfectly aligned. Phase components for TDBF are relatively aligned to that of the reference antenna element. Though the phase spectrum still fluctuates, its variation

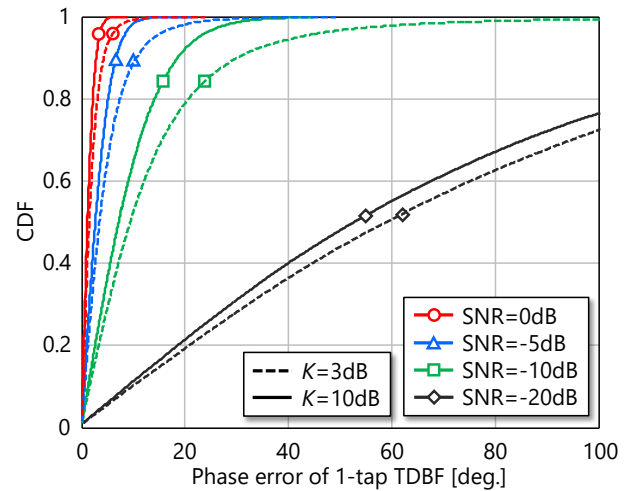


Figure 4: CDFs of phase error provided by 1-tap TDBF

is really quite small. This yields valuable beamforming performance as shown in Fig. 3 (a).

Fig. 4 plots CDFs of phase error provided by 1-tap TDBF. CDF performance is exhibited with various SNR and Rician K -factor. Assuming $N_s = 2048$, 1-tap TDBF weight calculation is performed via Eqs. (10) and (11) given SNR conditions. The absolute value of phase error (i.e. angle fluctuation of TDBF weight coefficient) is then obtained by difference from ideal case as $\text{SNR} = \infty$. Note that the SNR is indicated per antenna element, i.e. SISO case. Even though the noisy case such as $\text{SNR} = -10$ dB, phase error can be suppressed to ± 30 degrees, corresponding to 1 dB gain loss, with 90% probability.

These confirm that the 1-tap TDBF works well even though it is simple in manner. Though this paper assumes a Rician channel with larger K factor, millimeter wave signals are vulnerable to blockage caused by walls, humans, and so on. In practical environments, the LoS channel always does not exist. The proposed scheme can obtain the beamforming gain corresponding to the strongest and most stable arriving path if the LoS channel does not exist. This mechanism is completely the same as the existing beam training based approach which identifies the optimal beam pattern to achieve the largest gain. In addition, because we assume that several SAs are installed separately as shown Fig. 1, significant site diversity effect can be expected which will improve the probability that direct or quasi-direct paths exist. Table 1 summarizes computation complexities (defined here as the required number of complex multiplications). Here we assume that the number of available subcarriers for user data is N_c . Computation complexity of TDBF is simply derived

Table 1: Computation Complexity

Precoding scheme	Complexity
Proposed 1-tap TDBF	NtN_s
SVD	$2N_c(NtN_s^2 + N_s^3)$

as $NtNs$ from Eq. (11). That of SVD is taken to be $2NtNr^2 + 2Nr^3$ [27]. Eq. (11) involves only simple multiplications and its complexity is reasonable. On the other hand, SVD requires complex matrix calculation and the computation load becomes excessive in ultra-wideband communication. Results and Discussions

a) *System Level Simulation Settings*

Simulation parameters are listed in Table 2. BS is composed of 7 SAs, each of which is UPA with 121 antenna elements. As shown in Fig. 1, SAs are spaced at the interval of D . UEs are uniformly distributed in a circular cell with 20 m radius and inter-site distance (ISD) is fixed to 20 m. BS and UE heights are assumed to be 30 m and 1.5 m, respectively. In this evaluation model, SA selects one UE from its own cell to communicate with. Here, the user scheduling effect is simply taken into account by setting the minimum inter-UE distance to be 3 m. Assuming the Rician fading channel with $K = 10$ dB, the multipath component is modeled as 18 path exponential decay with 2 dB attenuation for each 10 ns in reference to the literature [28]. Free space propagation is assumed. Spatial correlation, i.e. $\mathbf{R}_{\alpha,j}$, $\mathbf{R}_{\alpha,i}$ and LoS channel, is also changed according to UE rotation on the horizontal plane as well as its location. CSI is updated every 1.3msec, which corresponds to 200 symbols for the 6.67 μ sec symbol duration. CSI estimation error due to receiver noise is excluded in order to evaluate the impact of the beamforming scheme. Transmission and reception weights are determined at each update event. TDBF weight is ideally obtained by correlation of channel impulse response, i.e. $\mathbf{v}'_m = \mathbf{h}_m^H \mathbf{h}_1$. This is validated in the Appendix. We compare 2 transmission schemes as follows;

- 1st eigenmode transmission per subcarrier
- Proposed 1-tap TDBF

Here we discuss the transmission beamforming performance of the two schemes above. UE is assumed to perform MRC reception per subcarrier regardless of the scheme.

b) *Simulation Results*

First we investigate how SA spacing impacts the spatial correlation. Cumulative distribution functions (CDFs) of SIR for all UEs are plotted in Fig. 5 for various values of SA spacing, D and Rician K -factor. The CDF plots also include subcarrier-by-subcarrier SIR. In this figure, red and blue lines show the results for 1-tap TDBF and 1st eigenmode, respectively. As this Fig. 4(a) shows, the performance gap between TDBF and 1st eigenmode is quite small and is almost negligible even though 1-tap TDBF is quite simple compared to the 1st eigenmode approach. Increasing D reduces the spatial correlation between SAs and thus SIR of more than 15 dB can be obtained without null steering. When $D = 20$ m, the SA spacing is equal to the radius of the circular

Table 2 : Simulation Parameters

Parameters	Values
Carrier frequency	20 GHz
Bandwidth	400 MHz
Number of FFT points; N_s	2048
Number of subcarriers; N_c	2000
Number of SA antenna elements; N_t	121 (11×11), UPA 0.5 λ spacing, HPBW=65°
Number of SAs; N_a	7
Number of UE antenna elements; N_r	16 (4×4), UPA 0.5 λ spacing, HPBW=65°
Number of UE; N_u	7
Number of stream per UE; N_s	1
Total Transmission power	0 dBm
Antenna gain	0 dBi
Noise power density	-174 dBm/Hz
Propagation model	Free space
Channel model	Rician fading, 18 path exponential decay RMS delay spread: 21.3nsec
Transmission / Reception Angular spread	5° / 5°
Precoding	1-tap TDBF / 1st eigenmode transmission
Post coding	MRC / 1st eigenmode reception
Symbol duration	6.67 μ sec
CSI estimation period	1.334 msec (200 symbol)
UE speed	10 km/h ($f_D T_s = 1.2 \times 10^{-3}$)

cell. Each cell is deeply overlapped and UE does not always access the nearest SA. Even in the severe situation, null steering is not necessary for multi-user MIMO communication in these two schemes. The SAs with massive antennas at BS side form narrow beams toward UEs since SAs have wider antenna aperture. Conversely, UEs use fewer number of antenna elements and so have narrow antenna aperture. Their main lobe may significantly impact neighboring SAs. Large D ensures beamforming gain of UE and improves SIR performance in this scheme.

Fig. 5(b) plots CDFs of SIR for $K = 3$ dB. Distribution characteristics of the 1st eigenmode transmission are almost the same as the case of $K = 10$ dB. SIR performance of TDBF is slightly degraded compared to 1st eigenmode transmission, especially for SIR values above 30 dB. This is because the phase misalignment of the TDBF weight for each subcarrier becomes large due to frequency selectivity when the effect of multipath component becomes more significant. In other words, the difference between TDBF and the 1st eigenmode transmission is negligible for SIR values under 30 dB. In millimeter wave communication,

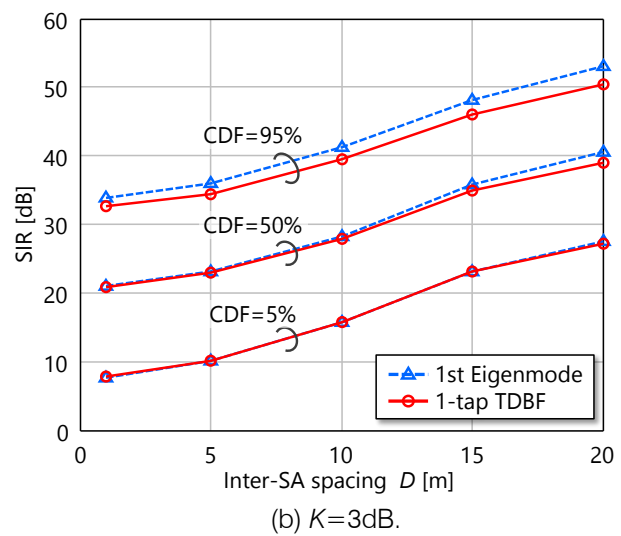
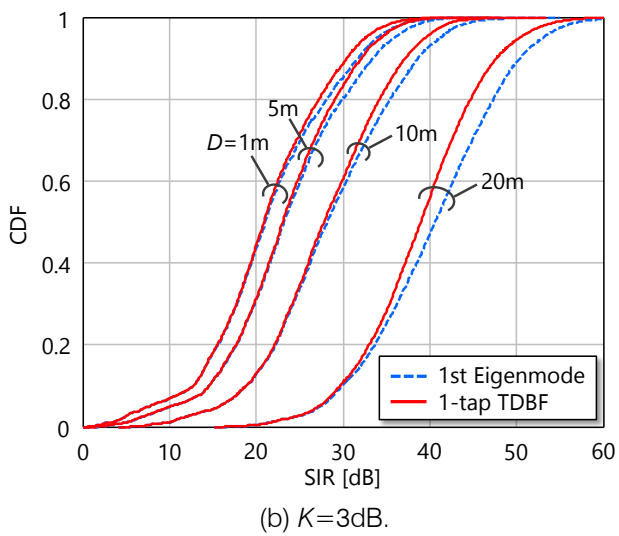
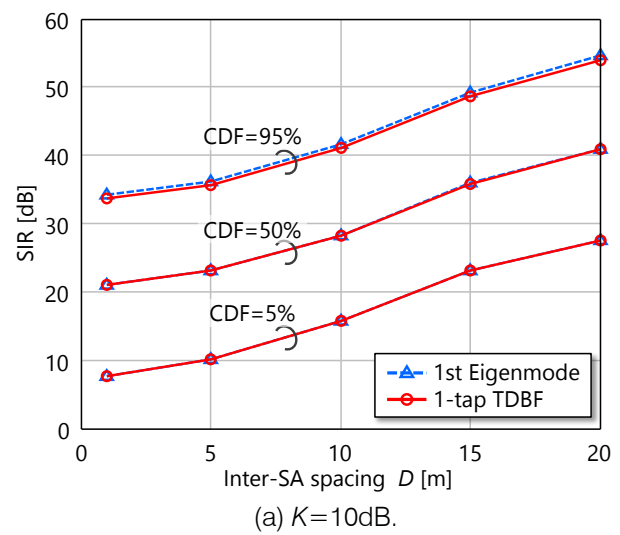
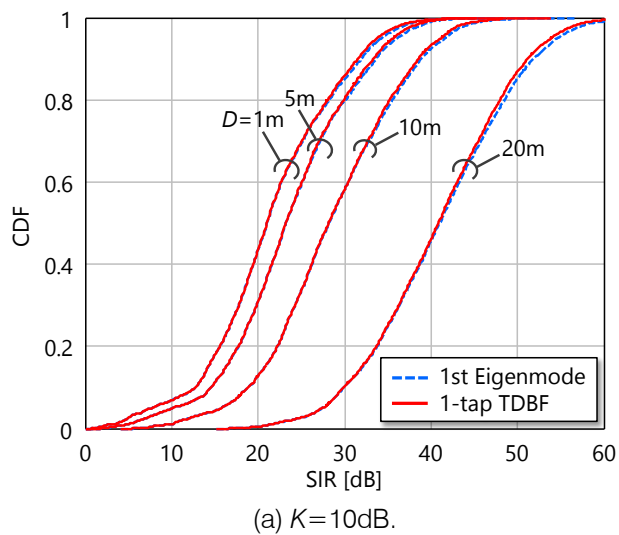


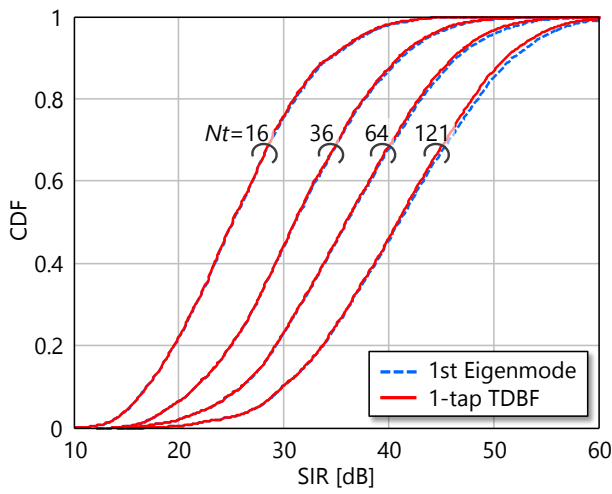
Figure 5 : CDFs of SIR with SA spacing

Figure 6 : SIR versus SA spacing

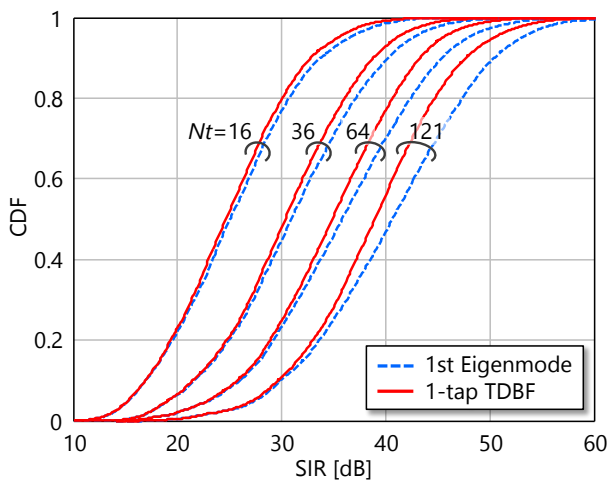
the link budget is poor and high SNR conditions of more than 30 dB cannot be usually expected. Moreover, the large time variation of the propagation channel may break the ideal communication condition. Therefore, TDBF and 1st eigenmode transmission have comparable practical performance even when $K = 3$ dB. Fig. 6 summarized each representative CDF value with SA spacing. As shown in these figures, enlarging SA spacing is effective in improving parallel transmission performance. In this evaluation model, SA has a small antenna aperture and its main lobe width is not narrow enough to separate UEs that are close neighbors. This inadequate user separation can be compensated by UE beamforming. Though each UE also forms a directional beam, its main lobe width is much wider than that of SA. To ensure user separation, SA spacing should be designed taking account of this effect. In ordinary multiuser MIMO communications, UEs are separated but antennas at BS side are closely installed. By dispersing the SAs, like the UEs, multiuser MIMO can be

operated effectively and simply. This is as new multiuser MIMO configuration. The following evaluations employ $D = 20$ m.

Fig. 7 plots CDFs of SIR with four transmission antenna element numbers per SA; $N_t = 16(4 \times 4)$, $36(6 \times 6)$, $64(8 \times 8)$, $121(11 \times 11)$. Rician K -factor is 10 dB or 3 dB. Note the total transmission power is constant for all N_t values. Increasing the number of antenna elements naturally contributes to enhance beamforming gain, so that SIR performance is rigorously improved. In the evaluation condition, cells are deeply overlapped since the cell radius and ISD are set to 20 m. This includes the situation that a UE does not access the nearest SA, desired signal can be greatly intensified due to the large beamforming gain with the large number of antenna elements. In addition, increasing the number of antenna elements enlarges the antenna aperture of SA. This narrows the main lobe width and improves user



(a) $K=10\text{dB}$.



(b) $K=3\text{dB}$.

Figure 7 : CDFs of SIR with number of SA antenna elements

isolation. These effects jointly contribute to obtaining the SIR improvement as presented.

As explained by Fig. 5, the SIR degradation of TDBF relative to the 1st eigenmode transmission can be seen at SIR values more than 30 dB. The performance gap tends to increase with SIR level because the slight phase misalignment of the TDBF weight cannot be ignored at such high SIR values. We introduced the additive noise effect and reevaluated CDFs of SINR performance; see Fig. 8. Using the parameters in Table 2, average SNR is obtained as -1 dB in the SISO case. Millimeter wave communication systems are deployed on the premise of lower SNR condition in SISO channels. Beamforming gain provided by UE/SA antenna array is calculated as $10\log_{10}(16 \times 121) = 32.9$ dB. This indicates that the performance discrepancy between 2 schemes becomes negligible in terms of SINR since SIR gaps larger than 30 dB are masked by the additive noise effect. By exploiting SA and UE beamforming with massive arrays, the expected desired

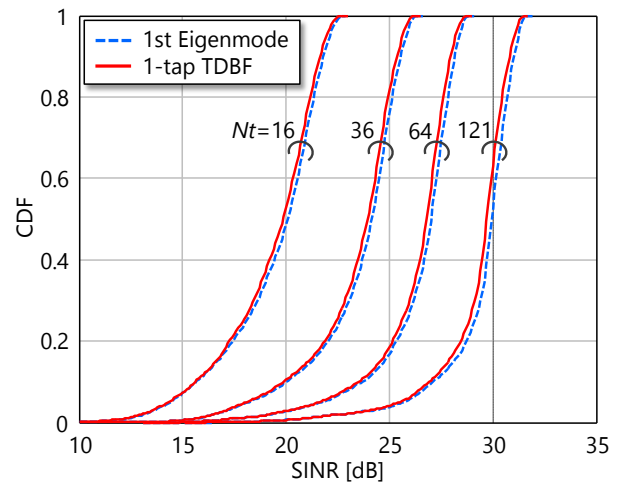


Figure 8 : CDFs of SINR with number of SA antenna elements ($D=20\text{m}$, $K=3\text{dB}$)

signal SNR level is raised to 30 dB. When UE correlation is small, its IUI level can be suppressed significantly under the noise level. The 1st eigenmode transmission cannot eliminate the IUI perfectly due to the absence of null steering. The slight phase misalignment of the TDBF weight also degrades the SIR performance, however, the degree of the phase misalignment is not so large. Therefore, the performance degradation by applying TDBF is negligible in the practical condition.

We evaluated in detail how far TDBF is affected by the NLoS component. CDF = 50% values of SI(N)R with Rician K -factor are plotted in Fig. 9. SIR performance for TDBF is largely degraded as the NLoS component becomes more predominant. However, TDBF can achieve $\text{SINR} = 28$ dB even with $K = 0$ dB while keeping its degradation relative to 1st eigenmode transmission to within 1 dB. This is still sufficient to provide higher throughput. This result verifies that our approach is effective even in multipath-rich channel environments.

Finally, SIR and SINR characteristics versus UE movement speed are presented. CDF = 5% and 50% value of SI(N)R are plotted in Fig. 10. The most significant feature of the present system embodiment is that SINR performance is basically not affected by UE movement, even in multiuser MIMO communication. In ordinary multiuser MIMO communication, UE movement tends to break null steering triggering significant IUI. As shown in this figure, however, the SIR performance of 1-tap TDBF and 1st eigenmode transmission are not degraded by UE movement. The origin of the good SIR performance of the 2 schemes is the spatial separation of transmission and reception antennas. This reduces the correlation between signal streams and makes null steering unnecessary. This feature offers the significant benefit of reducing the medium access control (MAC) overhead by extending CSI estimation interval. For example, N_v times expansion of UE movement speed is

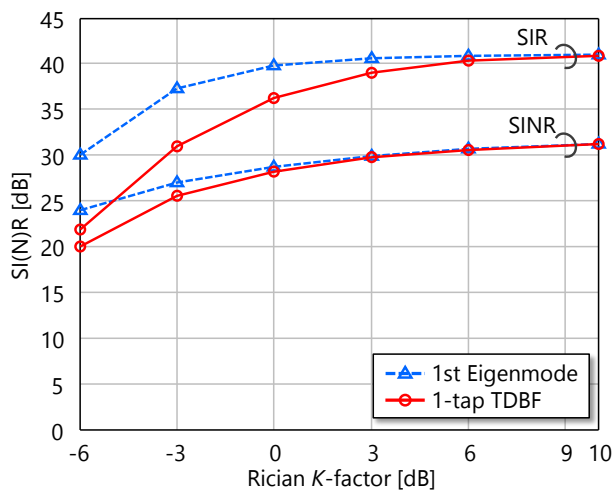


Figure 9 : CDF=50% value of SIR/SINR versus Rician K-factor ($D=20m, Nt=121$)

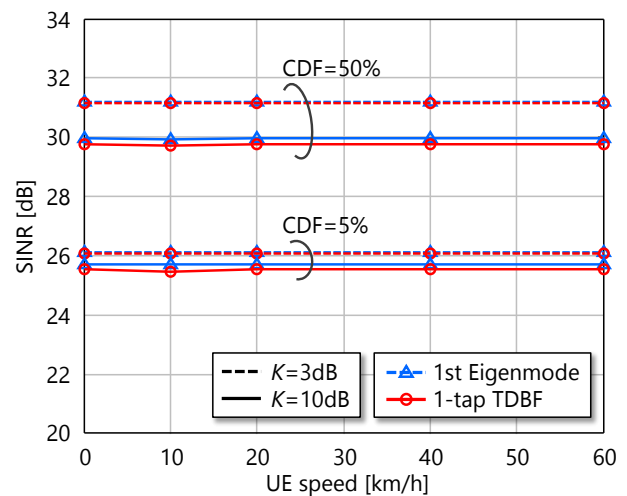


Figure 10 : CDF=5% and 50% values of SINR versus UE speed ($D=20m, Nt=121$)

equivalent to Nv times extension of CSI estimation interval. Therefore, if the expected UE speed is 4 km/h, it can be read from the figure that CSI estimation interval can be much longer, for example 15 fold, with no performance degradation, which represents a significant reduction in MAC overhead. Increasing the carrier frequency shortens the wavelength and strengthens the effect of UE movement. Meanwhile, separating SAs can de-correlate UEs and suppress the need for null steering in multiuser massive MIMO communications.

c) Discussions

For the heterogeneous networks in 5G, decoupling of the architecture control plane (C-plane) and user plane (U-plane) is assumed. With this assumption, all UEs can communicate with both small cell BS and macro cell BS. In a small cell environment, there is no guarantee of having a clear direct path between BS and UE, which may make the performance of our proposed scheme unstable. However, such UEs can communicate with the macro cell BS instead of the small cell BS. The probability of having direct path is expected to be increased by setting isolated SAs with location diversity. In order to effectively offload the traffic from a macro cell to a small cell, a lot of small cells should be scattered over crowded spaces. For this scenario, the deployment cost of the small cell BS should be reasonable, which emphasizes the value of the simplified operation of our proposal. Although our proposal is full digital 1-tap TDBF operation, it can be enhanced to analog BF with partial digital operation because the transmission and reception weights are constant across the bandwidth [8, 14-17]. This enhancement is also effective in reducing the cost as it needs fewer RF components. This paper assumed that each UE communicates with just a single SA, however, it is also possible for plural SAs to communicate with the same UE. In this case, though the correlation between streams for the same UE may become larger, it can be

compensated by reception side signal processing between the multiplexed chains. As the result, peak throughput per UE can be more than 10 Gbit/s which meets the 5G target requirement. Its validations will be further investigated.

As discussed above, our proposal has great advantages such as simple implementation and robustness against time varying channels in multiuser spatial multiplexing. It is an attractive candidate for small cell deployment in the 5G world.

IV. CONCLUSIONS

This paper verified the effectiveness of multiuser parallel transmission by SA beamforming on massive arrays assuming the LoS dominant channel environment in millimeter wavebands. Computer simulations revealed that valuable SINR gain can be stably attained without null steering when SAs are sufficiently separated in space. The proposal is also robust to channel time variation since null steering is not performed. Additionally, we proposed 1-tap TDBF, which can alleviate complex signal processing of the 1st eigenmode computation as well as suppressing the effect of additive noise on weight derivation. Our simplified and approximate approach achieved performance comparable to that of frequency domain 1st eigenmode transmission as the rigorous solution.

V. ACKNOWLEDGEMENT

The authors are sincerely grateful to Mr. Masashi Nakatsugawa and Mr. Hiroyuki Nakamura of NTT Access Network Service Systems Laboratories for their constant encouragement.

REFERENCES RÉFÉRENCES REFERENCIAS

1. Bangerter, B., Talwar, S., Arefi, R., & Stewart, K. (2014). Networks and devices for the 5G era. *IEEE Communications Magazine*, 52(2), 90-96. doi:10.1109/mcom.2014.6736748
2. Suyama, S., Shen, J., Benjebbour, A., Kishiyama, Y., & Okumura, Y. (2014). Super high bit rate radio access technologies for small cells using higher frequency bands. *2014 IEEE MTT-S International Microwave Symposium (IMS2014)*. doi:10.1109/mw sym.2014.6848637
3. Nakamura, T., Benjebbour, A., Kishiyama, Y., Suyama, S., & Imai, T. (2015). 5G Radio Access: Requirements, Concept and Experimental Trials. *IEICE Transactions on Communications*, E98. B(8), 1397-1406. doi:10.1587/transcom.e98.b.1397
4. Marzetta, T. L. (2010). Noncooperative Cellular Wireless with Unlimited Numbers of Base Station Antennas. *IEEE Transactions on Wireless Communications*, 9(11), 3590-3600. doi:10.1109/twc.2010.092810.091092
5. Hoydis, J., Brink, S. T., & Debbah, M. (2013). Massive MIMO in the UL/DL of Cellular Networks: How Many Antennas Do We Need? *IEEE Journal on Selected Areas in Communications*, 31(2), 160-171. doi:10.1109/jsac.2013.130205
6. Rusek, F., Persson, D., Lau, B. K., Larsson, E. G., Marzetta, T. L., & Tufvesson, F. (2013). Scaling Up MIMO: Opportunities and Challenges with Very Large Arrays. *IEEE Signal Processing Magazine*, 30(1), 40-60. doi: 10.1109/msp.2011.2178495
7. Larsson, E., Edfors, O., Tufvesson, F., & Marzetta, T. (2014). Massive MIMO for next generation wireless systems. *IEEE Communications Magazine*, 52(2), 186-195. doi:10.1109/mcom.2014.6736761
8. Obara, T., Suyama, S., Shen, J., & Okumura, Y. (2014). Joint fixed beamforming and eigenmode precoding for super high bit rate massive MIMO systems using higher frequency bands. *2014 IEEE 25th Annual International Symposium on Personal, Indoor, and Mobile Radio Communication (PIMRC)*. doi: 10.1109/pimrc.2014.7136237
9. Maruta, K., Iwakuni, T., Ohta, A., Arai, T., Shirato, Y., Kurosaki, S., & Iizuka, M. (2016). First Eigenmode Transmission by High Efficient CSI Estimation for Multiuser Massive MIMO Using Millimeter Wave Bands. *Sensors*, 16(7), 1051. doi:10.3390/s16071051
10. Spencer, Q., Swindlehurst, A., & Haardt, M. (2004). Zero-Forcing Methods for Downlink Spatial Multiplexing in Multiuser MIMO Channels. *IEEE Transactions on Signal Processing*, 52(2), 461-471. doi:10.1109/tsp.2003.821107
11. Taira, A., Iura, H., Nakagawa, K., Uchida, S., Ishioka, K., Okazaki, A., Okamura, A., Suyama, A., & Okumura, Y. (2015). Evaluation of Multi-Beam Multiplexing Technologies for Massive MIMO System Based on the EHF-band Channel Measurement. *2015 The 21st Asia-Pacific Conference on Communications (APCC)*.
12. Ogawa, Y., Yamaguchi, K., Bui, H. P., Nishimura, T., & Ohgane, T. (2013). Behavior of a Multi-User MIMO System in Time-Varying Environments. *IEICE Transactions on Communications*, E96.B(10), 2364-2371. doi:10.1587/transcom.e96.b.2364
13. Iwakuni, T., Maruta, K., Ohta, A., Shirato, Y., Kurosaki, S., Arai, T., & Iizuka, M. (2015). Massive MIMO effect for multiuser spatial multiplexing in time varying channel. *IEICE Communications Express*, 4(8), 270-275. doi:10.1587/comex.4.270
14. Tsang, Y. M., Poon, A. S., & Addepalli, S. (2011). Coding the Beams: Improving Beamforming Training in mmWave Communication System. *2011 IEEE Global Telecommunications Conference (GLOBECOM)*. doi:10.1109/glocom.2011.6134486
15. Alkhatieb, A., Ayach, O. E., Leus, G., & Heath, R. W. (2014). Channel Estimation and Hybrid Precoding for Millimeter Wave Cellular Systems. *IEEE Journal of Selected Topics in Signal Processing*, 8(5), 831-846. doi:10.1109/jstsp.2014.2334278
16. Lee, J., Gil, G., & Lee, Y. H. (2014). Exploiting spatial sparsity for estimating channels of hybrid MIMO systems in millimeter wave communications. *2014 IEEE Global Communications Conference (GLOBECOM)*. doi:10.1109/glocom.2014.7037320
17. Giordani, M., Mezzavilla, M., Barati, C. N., Rangan, S., & Zorzi, M. (2016). Comparative analysis of initial access techniques in 5G mmWave cellular networks. *2016 Annual Conference on Information Science and Systems (CISS)*. doi:10.1109/ciss.2016.7460513
18. Peter, M., Wisotzki, M., Raceala-Motoc, M., Keusgen, W., Felbecker, R., Jacob, M., Priebe, S., & Kurner, T. (2012). Analyzing human body shadowing at 60 GHz: Systematic wideband MIMO measurements and modeling approaches. *2012 6th European Conference on Antennas and Propagation (EUCAP)*. doi:10.1109/eucap.2012.6206013
19. Yu, K., Bengtsson, M., Ottersten, B., Mcnamara, D., Karlsson, P., & Beach, M. (2004). Modeling of Wide-Band MIMO Radio Channels Based on NLoS Indoor Measurements. *IEEE Transactions on Vehicular Technology*, 53(3), 655-665. doi:10.1109/tvt.2004.827164
20. Raj, J., Arokiasamy, S., Vikram, N., & Schoebel, J. (2008). Spatial Correlation and MIMO Capacity of Uniform Rectangular Dipole Arrays. *IEEE Antennas and Wireless Propagation Letters*, 7, 97-100. doi:10.1109/lawp.2008.919344
21. 3GPP TR 36.873 V12.2.0. (2015). Study on 3D Channel Model for LTE (Release 12). Retrieved August 12, 2016, from, <http://www.3gpp.org/dyna report/36873.htm>.

22. Cramer, R., Scholtz, R., & Win, M. (2002). Evaluation of an ultra-wide-band propagation channel. *IEEE Transactions on Antennas and Propagation*, 50(5), 561-570. doi:10.1109/tap.2002.1011221

23. Jakes, W. C. (1994). *Microwave mobile communications* (2nd ed.). New York: Wiley.

24. Tabata, T., Asato, H., Pham, D. H., Fujimoto, M., Kikuma, N., Hori, S., & Wada, T. (2007). Experimental study of adaptive array antenna system for ISDB-T high speed mobile reception. *2007 IEEE Antennas and Propagation International Symposium*. doi:10.1109/aps.2007.4395840

25. Nishimori, K., Cho, K., Takatori, Y., & Hori, T. (2001). Automatic calibration method using transmitting signals of an adaptive array for TDD systems. *IEEE Transactions on Vehicular Technology*, 50(6), 1636-1640. doi:10.1109/25.966592

26. Fukuzono, H., Murakami, T., Kudo, R., Takatori, Y., & Mizoguchi, M. (2015). Weighted-Combining Calibration on Multiuser MIMO Systems with Implicit Feedback. *IEICE Transactions on Communications*, E98.B(4), 701-713. doi:10.1587/transcom.e98.b.701

27. Trefethen, L. N., & Bau, D. (1997). *Numerical linear algebra*. Philadelphia: Society for Industrial and Applied Mathematics.

28. Deng, S., Samimi, M. K., & Rappaport, T. S. (2015). 28 GHz and 73 GHz millimeter-wave indoor propagation measurements and path loss models. *2015 IEEE International Conference on*

Communication Workshop (ICCW). doi:10.1109/iccw.2015.7247348

APPENDIX

Defining the channel impulse response as;

$$\mathbf{h}_m = [h_m[0] \ h_m[1] \ \dots \ h_m[L-1] \ 0 \ \dots \ 0]^T \quad (A1)$$

1-tap TDBF weight coefficient ideally approaches $v'_m = \mathbf{x}_m^H \mathbf{x}_1 / N_s \approx \mathbf{h}_m^H \mathbf{h}_1$ and we utilized this value in the simulations. From Eq. (A1), Eq. (10) can be rewritten as;

$$\mathbf{x}_m = [\mathbf{C}^0 \mathbf{h}_m \ \mathbf{C}^1 \mathbf{h}_m \ \dots \ \mathbf{C}^{N_s-1} \mathbf{h}_m] \mathbf{s} \quad (A2)$$

where $\mathbf{s} = [s_0, \dots, s_{N_s-1}]^T \in \mathbb{C}^{N_s \times 1}$. The AWGN term is omitted for simplicity. \mathbf{C} is defined as the row-wise cyclic shift operator;

$$\mathbf{C} = \begin{bmatrix} 0 & 1 & 0 & \dots & 0 \\ & 0 & 1 & & \\ \vdots & \vdots & 0 & \ddots & \vdots \\ 0 & & & & 1 \\ 1 & 0 & 0 & \dots & 0 \end{bmatrix} \quad (A3)$$

\mathbf{C}^α performs cyclic shift operation α -times and has the following characteristic;

$$(\mathbf{C}^\alpha)^H = \mathbf{C}^{-\alpha} \quad (A4)$$

Eq. (11) can be derived as follows,

$$\begin{aligned} v'_m &= \frac{1}{N_s} \mathbf{x}_m^H \mathbf{x}_1 \\ &= \frac{1}{N_s} \mathbf{s}^H [\mathbf{C}^0 \mathbf{h}_m \ \mathbf{C}^1 \mathbf{h}_m \ \dots \ \mathbf{C}^{N_s-1} \mathbf{h}_m]^H [\mathbf{C}^0 \mathbf{h}_1 \ \mathbf{C}^1 \mathbf{h}_1 \ \dots \ \mathbf{C}^{N_s-1} \mathbf{h}_1] \mathbf{s} \\ &= \frac{1}{N_s} \mathbf{s}^H \begin{bmatrix} (\mathbf{C}^0 \mathbf{h}_m)^H \mathbf{C}^0 \mathbf{h}_1 & (\mathbf{C}^0 \mathbf{h}_m)^H \mathbf{C}^1 \mathbf{h}_1 & \dots & (\mathbf{C}^0 \mathbf{h}_m)^H \mathbf{C}^{N_s-1} \mathbf{h}_1 \\ (\mathbf{C}^1 \mathbf{h}_m)^H \mathbf{C}^0 \mathbf{h}_1 & \ddots & & \\ \vdots & & (\mathbf{C}^\alpha \mathbf{h}_m)^H \mathbf{C}^\beta \mathbf{h}_1 & \vdots \\ (\mathbf{C}^{N_s-1} \mathbf{h}_m)^H \mathbf{C}^0 \mathbf{h}_1 & \dots & \dots & (\mathbf{C}^{N_s-1} \mathbf{h}_m)^H \mathbf{C}^{N_s-1} \mathbf{h}_1 \end{bmatrix} \mathbf{s} \\ &= \frac{1}{N_s} [s_0^* \ \dots \ s_\alpha^* \ \dots \ s_{N_s-1}^*] \begin{bmatrix} \mathbf{h}_m^H \mathbf{C}^0 \mathbf{h}_1 & \mathbf{h}_m^H \mathbf{C}^1 \mathbf{h}_1 & \dots & \mathbf{h}_m^H \mathbf{C}^{N_s-1} \mathbf{h}_1 \\ \mathbf{h}_m^H \mathbf{C}^{-1} \mathbf{h}_1 & \ddots & & \\ \vdots & & \mathbf{h}_m^H \mathbf{C}^{\beta-\alpha} \mathbf{h}_1 & \vdots \\ \mathbf{h}_m^H \mathbf{C}^{-N_s+1} \mathbf{h}_1 & \dots & \dots & \mathbf{h}_m^H \mathbf{C}^0 \mathbf{h}_1 \end{bmatrix} \begin{bmatrix} s_0 \\ \vdots \\ s_\beta \\ \vdots \\ s_{N_s-1} \end{bmatrix} \\ &= \frac{1}{N_s} \sum_{\alpha=0}^{N_s-1} s_\alpha^* s_\alpha \mathbf{h}_m^H \mathbf{h}_1 + \frac{2}{N_s} \sum_{\alpha=0}^{N_s-2} \sum_{\beta=\alpha+1}^{N_s-1} \text{Re} (s_\alpha^* s_\beta \mathbf{h}_m^H \mathbf{C}^{\beta-\alpha} \mathbf{h}_1) \end{aligned} \quad (A5)$$

If N_s is large enough, we can expect,

$$E[s_\alpha^* s_\beta] = \begin{cases} 1 & \text{for } \alpha = \beta \\ 0 & \text{for } \alpha \neq \beta \end{cases} \quad (\text{A6})$$

In addition,

$$\mathbf{h}_m^H \mathbf{C}^{\beta-\alpha} \mathbf{h}_1 = 0 \quad \text{for } \beta - \alpha > L \quad (\text{A7})$$

Therefore, the absolute value of the 2nd term in Eq. (A5) becomes much smaller than that of the 1st term. The following result can be derived;

$$v'_m \approx \mathbf{h}_m^H \mathbf{h}_1 \quad (\text{A8})$$



GLOBAL JOURNALS INC. (US) GUIDELINES HANDBOOK 2016

WWW.GLOBALJOURNALS.ORG